Digital Signal Processing 60 (2017) 46–55

Contents lists available at ScienceDirect

Digital Signal Processing

www.elsevier.com/locate/dsp

Attenuation estimation using high resolution time–frequency transforms

Jean Baptiste Tary [a,b,*], Mirko van der Baan [a], Roberto Henry Herrera [a]

[a] Department of Physics, University of Alberta, Edmonton, Canada
[b] Departamento de Geociencias, Universidad de Los Andes, Bogotá, Colombia

ARTICLE INFO

Article history:
Available online 26 August 2016

Keywords:
Attenuation
Synchrosqueezing transform
Basis pursuit
Empirical mode decomposition
Peak frequency
Time–frequency

ABSTRACT

Wave attenuation is often measured using spectral techniques such as the spectral ratio method and the frequency shift method, comparing the spectral content of pairs of waveforms along the ray path. The recent introduction of novel highly-localized time–frequency transforms leads to high-resolution but discontinuous spectra. It prevents the use of these time–frequency transforms with conventional attenuation measurement methods. We show how three highly-localized time–frequency transforms, namely basis pursuit, the synchrosqueezing wavelet transform, and complete ensemble empirical mode decomposition, can still be used to estimate attenuation using the peak frequency method. Assuming a Ricker source wavelet, the decrease in peak frequency of a wave spectrum as it propagates in a given medium is used to estimate attenuation. When applied to a synthetic benchmarking signal corrupted by Gaussian white noise, the three transforms show different degrees of performance and robustness for different signal-to-noise ratios. The developed methodology is suitable for geophysical investigations, but may also find application in other fields such as biomedicine, acoustics and engineering.

1. Introduction

Attenuation refers to the loss of energy as a wave propagates through a given medium. In the case of seismic waves in the Earth, attenuation is usually separated into intrinsic losses, connected to the conversion of seismic energy into heat or fluid flow [32], and apparent attenuation corresponding to various physical processes such as scattering effects [34]. Intrinsic attenuation is connected to various medium and fluid properties such as fluid content, viscosity, and permeability [5], which makes it a potential monitoring tool (e.g., [36,6]). Attenuation measurements have also a wide range of applications outside of geophysics, such as in acoustics [22,17], biomedicine [2], archeology [21], astrophysics [28] or engineering [27,9].

For a propagating wavelet, the quality factor Q is commonly defined as the total wave energy divided by the loss of energy per cycle. Attenuation, inversely proportional to the quality factor, is assumed to be approximately constant in the frequency band relevant for seismic waves in the Earth [29]. However, higher frequencies decay more rapidly than lower frequencies simply because attenuation corresponds to a certain absorption value per signal period [42]. The disappearance of higher frequencies leads to a shift of the dominant frequency toward lower frequencies and a relative widening of its main lobe (Fig. 1a, b).

Attenuation can then be measured either in the time domain, using the amplitude decay of signals with distance/time, or in the frequency domain by quantifying spectral changes. The two main spectral methods are the spectral ratio method and the frequency shift method [33]. Both operate by comparing the spectra of a pair of arrivals, for instance at different locations along the ray path. Several other methods were developed to estimate quality factors from a single frequency estimate, such as the peak frequency method [48] and the analytical signal method [42,14]. The peak frequency information should be preserved by highly-localized time–frequency transforms, even though bandwidth information is lost.

New highly-localized time–frequency transforms representations were developed recently, such as basis pursuit (BP) [10], empirical mode decomposition [25] and the synchrosqueezing wavelet transform (SST) [12]. See Tary et al. [38] for more background on their rationales and performances. High-resolution time–frequency transforms improve the readability of time–frequency representation by focusing the spectral information around the main frequency content of the signal. This can be useful in a variety of applications, encompassing climate time series [40], solar physics [1], seismic data analysis [50,24], and signal denoising [45]. The high spectral localization, on the other hand, prevents or compli-

* Corresponding author.
E-mail address: jb.tary@uniandes.edu.co (J.B. Tary).

http://dx.doi.org/10.1016/j.dsp.2016.08.007
1051-2004/

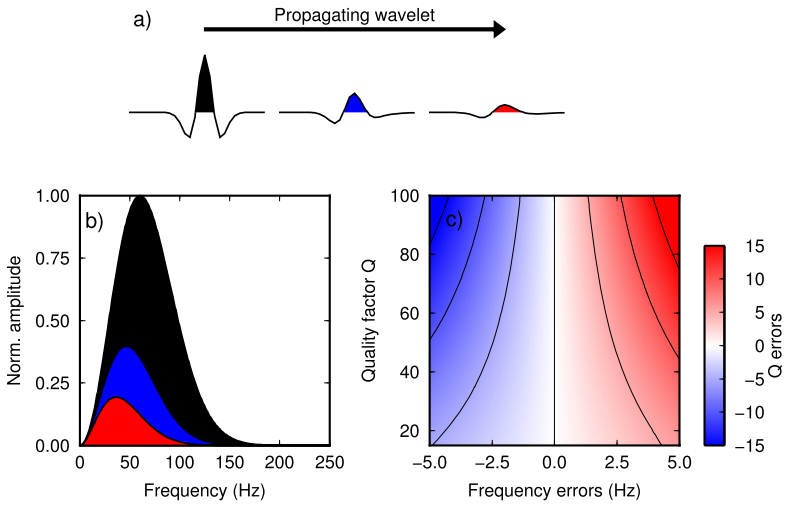

Fig. 1. a) Waveforms of a source Ricker wavelet with a peak frequency of 60 Hz (black) and two attenuated wavelets after 0.25 (blue) and 0.5 s (red) propagation time using a quality factor of 45. The wavelets are sampled at 500 Hz. b) Normalized Fourier spectra of the three wavelets shown in a). c) Errors in quality factor Q estimations due to errors in peak frequency, using the peak frequency method of Zhang and Ulrych [48] and different quality factors. The black lines correspond to Q error contours (increments of 5). We first use eq. (3), a source peak frequency of 60 Hz, and a given quality factor to estimate theoretical peak frequencies. An error is then introduced in these values in the range between −5 and 5 Hz, and the quality factor is computed using eqs. (4) and (5). The true quality factors are then subtracted from the quality factor estimations to get the Q errors. (For interpretation of the references to color in this figure legend, the reader is referred to the web version of this article.)

cates the use of the most common spectral estimation techniques for attenuation measurements since these often require either a continuous spectrum or a bandwidth estimate [42].

In principle, attenuation could still be estimated by high-resolution time–frequency transforms using the peak frequency technique. In the following, we first describe the peak frequency technique and three time–frequency transforms: BP, SST and empirical mode decomposition. We then test the performance of the peak frequency method in combination with these three high-resolution time–frequency transforms for accurate and precise attenuation estimation using a controlled synthetic experiment.

2. Quality factor estimation

The amplitude spectrum of a signal recorded at a given receiver $A_R(f)$ can be approximated as a multiplication of the source amplitude spectrum $A_S(f)$, amplitude modifications due to transmission/reflection at interfaces in addition to instrument and medium responses $G(t, f)$ (e.g., geometric spreading, source/instrument transfer function, radiation pattern), and attenuation [33], producing

$$A_R(t, f) = G(t, f)\, A_S(f)\, \mathrm{e}^{-\frac{\pi f t}{Q}}, \tag{1}$$

where f is frequency, t the travel-time and Q the quality factor grouping all sources of attenuation. We then assume that the attenuation is constant between the source and the receiver, and that $G(t, f)$ has no significant influence on the receiver spectrum in the frequency band of interest.

The individual arrivals are represented using the Ricker wavelet spectrum given by:

$$A_S(f) = \frac{2}{\sqrt{\pi}} \frac{f^2}{f_0^3} \mathrm{e}^{\frac{-f^2}{f_0^2}}, \tag{2}$$

with f_0 the peak frequency of the Ricker wavelet. Equating the derivative of eq. (1) with respect to frequency to 0 and using the Ricker spectrum as the source spectrum, the peak frequency f_p of latter arrivals after attenuation is [48]

$$f_p = f_0^2 \left[\sqrt{\left(\frac{\pi t}{4Q}\right)^2 + \left(\frac{1}{f_0}\right)^2} - \frac{\pi t}{4Q} \right]. \tag{3}$$

Eq. (3) is then used to estimate quality factors. The change in peak frequencies between signals is directly related to the quality factor by

$$Q = \frac{\pi t f_p f_0^2}{2\left(f_0^2 - f_p^2\right)}. \tag{4}$$

In addition, the peak frequency of the source wavelet[1] f_0 can be determined using the peak frequencies at two different times using

$$f_0 = \sqrt{\frac{f_{p1} f_{p2} \left(t_2 f_{p1} - t_1 f_{p2}\right)}{t_2 f_{p2} - t_1 f_{p1}}}, \tag{5}$$

for wavelets recorded at times t_1 and t_2 with peak frequencies f_{p1} and f_{p2}. This also assumes constant attenuation between measurements at times t_1 and t_2.

The peak frequency method for estimating Q is relatively sensitive to systematic errors in peak frequency estimations (see Fig. 1c). Systematic errors toward higher frequencies for example, for the same travel-time and frequency difference between wavelets, lead to quality factor overestimations because higher frequencies are attenuating faster compared with lower frequencies. The method is also more sensitive for higher quality factors since peak frequency changes are smaller compared to those arising from lower quality factors for identical propagation times. For example, considering quality factors comprised between 15 and 100, a peak frequency for the source wavelet of 60 Hz, and attenuated wavelets after a propagation time of 0.25 and 0.5 s, the errors in quality factor range between −9 and 9.4 in the case of an error of ±2.5 Hz (Fig. 1c). In the case of multiple layers, the quality factors are estimated successively from layer to layer by layer stripping (see Zhang and Ulrych [48] for more details). Errors in the estimations of quality factors from previous layers are then propagated to those of the following layers.

[1] For clarification, the source wavelet is the initial wavelet at the point of origin and the observed wavelet is the recorded wavelet after it has propagated over some distance. These terms should not be confused with the mother wavelet, that is, the template used in continuous wavelet transforms or associated time–frequency transforms.

3. High-resolution time–frequency transforms

3.1. Basis pursuit

BP is a sparse time–frequency technique based on the selection of time–frequency atoms from a user defined dictionary [10,38]. This corresponds to the inner product of a signal $s(t)$ with atoms ψ_γ as $\langle s(t), \psi_\gamma \rangle$, γ corresponding to atom parameters varying within the dictionary. Since these parameters also include time shifts, this technique assumes that a given signal $\mathbf{s}$ can be represented by a convolution model between a set of atoms $\mathbf{\Psi}$ and a set of coefficients $\mathbf{a}$, which represent template waveforms and a reflectivity series in our case, respectively, plus some additive random noise $\mathbf{n}$. Using matrix formalism, this corresponds to

$$\mathbf{s} = \mathbf{\Psi a} + \mathbf{n} = \begin{pmatrix} \mathbf{\Psi_1} & \mathbf{\Psi_2} & \cdots & \mathbf{\Psi_N} \end{pmatrix} \begin{pmatrix} a_1 \\ a_2 \\ \vdots \\ a_N \end{pmatrix} + \mathbf{n}, \tag{6}$$

where N is the number of templates in the dictionary.

In the case of the BP denoising algorithm, the atom selection process is optimized through an iterative inversion scheme [50,8]. The cost function J balances data misfit (ℓ_2 norm) and the number of non-zero time–frequency coefficients (ℓ_1 norm scaled by a regularization parameter λ) as

$$J = \|\mathbf{s} - \mathbf{\Psi a}\|_2^2 + \lambda \|\mathbf{a}\|_1. \tag{7}$$

The sparsity is imposed by the ℓ_1 term in eq. (7) which favors solutions with fewer higher amplitude coefficients compared with solutions based on the ℓ_2 regularization norm. Eq. (7) has no closed form solutions; the final result is obtained iteratively using the Fast Iterative Soft Thresholding Algorithm (FISTA) [3,8]. Dictionaries that can be employed with BP are very diverse [10]. They should contain atoms that can match the signal under investigation. We build complex wavelet dictionaries by computing the analytic signal of wavelets for a predefined range of frequencies [7] using the Hilbert transform. The initial set of coefficients $\mathbf{a}$ is then obtained using the continuous wavelet transform. The time–frequency distribution is finally thresholded iteratively using soft thresholding in the time–frequency domain using the continuous wavelet transform for faster implementation. See Vera Rodriguez et al. [45] and Bonar and Sacchi [8] for more details.

3.2. Synchrosqueezing transform

The SST is a technique based on the combination of time–frequency methods followed by a reassignment step. SST can be based on the short-time Fourier transform [39], the S-transform [26], the wave packet transform [18], or the continuous wavelet transform [12,40], which is the one used on this study. This technique combines the advantages of variable time–frequency resolution with smearing reduction [38].

The SST assumes that the non-stationary signal under investigation $s(t)$ is the sum of K well-separated and smoothly varying frequency components,

$$s(t) = \sum_{k=1}^{K} A_k(t) \cos(2\pi\theta_k(t)) + n(t), \tag{8}$$

where t is time, $A_k(t)$ and $\theta_k(t)$ the instantaneous amplitude and phase of the kth component, respectively, and $n(t)$ some random noise. Instantaneous frequencies (IF) are then $f_k = \frac{1}{2\pi}\frac{\mathrm{d}\theta_k(t)}{\mathrm{d}t}$. The continuous wavelet transform representation $W_s(a,b)$ of signal $s(t)$ is given by

$$W_s(a,b) = \frac{1}{\sqrt{a}} \int_{-\infty}^{\infty} s(t)\, \psi^* \left(\frac{t-b}{a} \right) \mathrm{d}t, \tag{9}$$

where ψ is the mother wavelet and ψ^* its complex conjugate, scaled and time-shifted by a and b, respectively. As for BP, this also corresponds to the inner product between a signal $s(t)$ and template waveforms, which are stretched and time-shifted versions of the mother wavelet, as $\langle s(t), \frac{1}{\sqrt{a}}\psi(\frac{t-b}{a}) \rangle$ [31]. In order to reduce the smearing along the scale axis, Daubechies et al. [12] proposed to reassign the non-zero coefficients of $W_s(a,b)$ to the IFs $\omega_s(a,b)$ following,

$$\omega_s(a,b) = \frac{-\mathrm{i}}{2\pi W_s(a,b)} \frac{\partial W_s(a,b)}{\partial b}, \tag{10}$$

where i is the imaginary number. The representation $W_s(a,b)$ is then reassigned to $(\omega_s(a,b), b)$ in the time–frequency plane. In practice the number of meaningful frequency components is determined by a threshold acting on the continuous wavelet transform representation. This threshold is especially important to correctly identify the peak frequencies of signals with low signal-to-noise ratio. We set up the thresholding by dividing the strongest frequency component by a given value. For example, for a value of 2, all frequency components having half the maximum amplitude or less are disregarded (i.e., set to zero). This corresponds to a threshold of 50% of the maximum amplitude of continuous wavelet transform representations. For the application to the synthetic signal, we present peak frequencies and quality factor estimates using dividing values of 1.25, 2, 4 and 10, which correspond to thresholds at 80, 50, 25 and 10%, respectively.

3.3. Variants of empirical mode decomposition

Empirical mode decomposition is applied directly on the time domain signal. Extrema (minima and maxima) of the signal are interpolated to obtain the upper and lower envelopes. The mean of these two envelopes is then subtracted from the signal. This process is repeated until the number of zero-crossings and extrema in the residue differs by at most one and the local mean is zero. The residue is then considered as an intrinsic mode function (IMF) and subtracted from the signal. The same process is repeated until the signal is close to zero everywhere or monotonic [25,20]. This process is called *sifting*.

IMFs are then extracted recursively from the signal, beginning with the highest frequency one [25]. The time–frequency representation corresponding to these IMFs is obtained by computing the IFs for each of them via the Hilbert spectrum [25]. The extracted IMFs are narrow-band and symmetric leading to smooth and positive IFs. Empirical mode decomposition decomposes completely the signal, meaning that the signal can be reconstructed by summing all the IMFs. The IMFs are quasi-orthogonal to each other limiting mode mixing between IMFs [16,4]. This produces highly localized time–frequency distributions.

Two extensions of empirical mode decomposition, namely ensemble empirical mode decomposition (EEMD) [46] and complete ensemble empirical mode decomposition (CEEMD) [43], address some of the problems of empirical mode decomposition such as mode mixing and aliasing using the injection of Gaussian white noise of small amplitude. As the same sifting process is carried out for a given number of noise realization independently, and then averaged, EEMD decompositions sometimes lead to different IMF numbers for different noise realizations, and some noise can migrate to the IMFs [43]. In addition, the EEMD technique can lead to an incomplete decomposition of the signal [20]. With CEEMD, the IMFs are once again calculated successively [43] and lead to a complete decomposition of the signal. However, some noise can

Table 1
Peak frequencies f_p for the source wavelet (f_0) and the 6 wavelets of the synthetic signal computed by the Fourier transform on the noiseless synthetic signal (reference), and the synthetic signal plus noise (raw and smoothed Fourier spectra).

	Reference meas.			Raw Fourier spectra						Smoothed Fourier spectra					
	t[a] (s)	f_p (Hz)	Q[b]	$\bar{f}_p$[c]	$\tilde{f}_p$[d]	σ_{f_p}[e]	$\bar{Q}$[c]	$\tilde{Q}$[d]	σ_Q[e]	$\bar{f}_p$[c]	$\tilde{f}_p$[d]	σ_{f_p}[e]	$\bar{Q}$[c]	$\tilde{Q}$[d]	σ_Q[e]
f_0	0	60													
f_{p1}	0.25	50.8	70	50.6	51.3	3.9	158.7	71.7	271.3	50.7	50.7	1.3	74.3	68.5	16.4
f_{p2}	0.50	43.2	70	43.8	43.5	4.6	178.3	74.9	261.0	43.2	43.0	2.0	74.6	69.6	17.3
f_{p3}	0.75	37.1	70	37.3	37.0	4.5	162.0	65.3	295.7	37.2	36.9	2.3	74.5	70.0	16.1
f_{p4}	1.00	29.6	45	31.4	31.3	5.0	63.2	39.3	485.6	29.6	30.0	2.7	56.2	47.5	28.8
f_{p5}	1.25	24.4	45	26.4	26.5	7.1	61.2	48.0	887.8	24.7	24.1	3.2	54.9	46.6	28.7
f_{p6}	1.50	20.5	45	45.2	22.0	93.0	15.6	35.6	554.2	20.8	20.2	3.7	54.2	42.1	34.1

[a] Travel-times from the source to the recording time.
[b] Theoretical quality factors Q in the corresponding layers (see Fig. 2a).
[c] Mean variables.
[d] Median variables.
[e] Standard deviations.

also migrate to the IMFs and some spurious IMFs can appear [11]. Because of the stochastic nature of noise injection, frequency estimates obtained using the same method and procedure may yield slightly different results.

4. Application to a synthetic signal

A synthetic signal is created by calculating the effects of dispersion and attenuation on a unit impulse propagating in a layered medium with different quality factors [44]. The resulting medium response is then convolved with the source wavelet. For the present synthetic signal, the source wavelet is a Ricker wavelet with a peak frequency of 60 Hz and the medium consists of two domains with quality factors of 70 and 45 for the first and second domains, respectively (Fig. 2a). The final synthetic signal consists then of three reflections per domain, corresponding to attenuated Ricker source wavelets, at different propagation times (see Fig. 2b,c and Table 1). This is equivalent to a 6-layer model over a half-space, with the first three layers in the first Q-domain with a value of 70, and the next three layers in the second Q-domain with a value of 45.

Each wavelet, which has a duration of ~0.1 s, is extracted from the 2 s-long noiseless synthetic trace, and extended to a 0.5 s-long signal by zero-padding to reduce edge and wrap-around artefacts in the transforms. Random Gaussian white noise is then added to the 6 wavelets, with maximum amplitude corresponding to different signal-to-noise ratio (SNR) depending on the wavelet (Fig. 2). The wavelet amplitudes range from 0.07 for the first wavelet to 0.0026 for the last wavelet because of amplitude losses due to attenuation. Using the following definition for the SNR

$$SNR = 20\log_{10}\left(\frac{S_a}{N_a}\right), \tag{11}$$

where S_a and N_a are the maximum amplitude of the wavelet and the random noise, respectively, the SNR roughly ranges from 30 dB for the first wavelet to 0 dB for the last wavelet. The wavelets are finally windowed by a Tuckey window, reducing the random noise contribution outside the wavelet's time support.

One peak frequency is extracted per wavelet corresponding to the frequency of maximum amplitude. As peak frequency measurements can vary depending on the random noise, we calculate peak frequencies and quality factors for 50 realizations of random noise. In the following, we present the mean, median and standard deviation of peak frequencies and quality factors estimations for the best sets of parameters obtained for each transform.

4.1. Reference: Fourier transform

The Fourier transform is also applied to the noiseless synthetic signal in order to obtain reference estimations of the peak frequencies of the observed wavelets (see Table 1). For the random noise realizations, we show two sets of estimations: with or without smoothing the Fourier spectra. We apply a 6-pole low-pass butterworth filter to smooth the initial spectra.

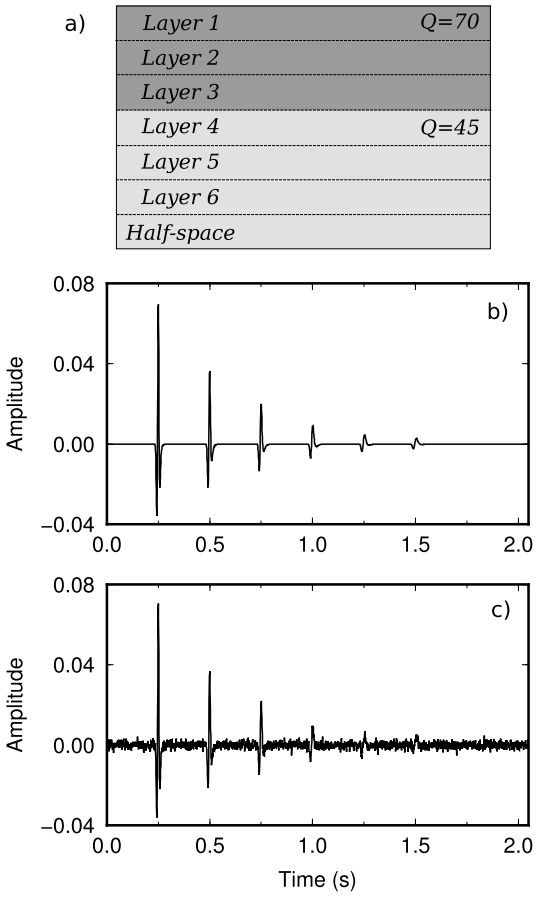

Fig. 2. Synthetic signal consisting of 6 Ricker wavelets attenuated using different quality factors (see model in a) and Table 1), without (b)) and with (c)) Gaussian white noise. The source wavelet is a Ricker wavelet with a peak frequency of 60 Hz. The signal is sampled at 1000 Hz.

Without smoothing, the mean and median peak frequencies estimated are close to the reference ones but show large standard deviations of several hertz or more. Median estimates are generally more accurate than mean estimates as in the case of the peak frequency of the last wavelet for example (Table 1). After smoothing, standard deviations are greatly reduced especially when the amount of noise is important. Various attempts were made to improve the peak frequency estimation using the Fourier transform,

Table 2
Reference measurements using the Fourier transform (see Table 1) and peak frequencies and quality factors estimations using basis pursuit (BP) with a Ricker wavelet dictionary and a regularization parameter $\lambda = 4$. See Table 1 for meaning of symbols.

	Reference meas.			BP estimations with $\lambda = 4$					
	t (s)	f_p (Hz)	Q	$\bar{f}_p$	$\tilde{f}_p$	σ_{f_p}	$\bar{Q}$	$\tilde{Q}$	σ_Q
f_{p1}	0.25	50.8	70	48.4	48.5	0.4	79.6	79.7	5.2
f_{p2}	0.50	43.2	70	42.4	42.4	0.6	80.2	80.3	4.9
f_{p3}	0.75	37.1	70	37.0	36.9	0.9	78.8	78.3	5.7
f_{p4}	1.00	29.6	45	30.5	30.5	1.5	50.4	49.0	11.0
f_{p5}	1.25	24.4	45	24.9	24.9	2.1	47.9	46.7	12.8
f_{p6}	1.50	20.5	45	20.6	21.0	2.5	45.7	44.7	11.6

such as filtering the signal prior to the computations, using averaged spectra obtained through the Welch method, and selecting only a useful frequency range by setting up an amplitude threshold on the averaged spectra, but none of these attempts improved significantly the peak frequency estimations compared with those using the smoothed spectra. Likewise, use of more complex windowing tapers such as multi-taper ones [41] are not thought to change our general conclusions.

4.2. Basis pursuit

In the case of this synthetic signal, we use either Ricker or Morlet wavelet dictionaries, and different number of iterations (i.e., 80, 100, 150) and regularization parameters λ (i.e., 0.5, 1, 2, 4, 8). The dictionaries are obtained using the continuous wavelet transform [7] with a linear frequency axis ranging from 2 to 500 Hz. The main impact of the number of iterations and the regularization parameter is on the amount of thresholding applied to the time–frequency representation. As both parameters have similar effects, we here use 100 iterations and different regularization parameters λ to show the effect of thresholding on the peak frequency estimations. Increasing the regularization parameter penalizes more the number of non-zero time–frequency coefficients during the inversion, leading to sparser representations.

Peak frequency estimation using BP is dependent on a trade-off between noise amplitude and amount of thresholding. Without enough thresholding, peak frequencies for signals with low signal-to-noise ratio could actually correspond to the noise, whereas over-thresholding might also bias peak frequency estimation toward lower frequencies (see Fig. 3). Using the Ricker wavelet dictionary and an appropriate level of thresholding, BP provides peak frequencies that are very close to the reference ones with little standard deviations (Table 2).

On the other hand, with the Morlet wavelet dictionary, even though peak frequencies are close to the reference ones, their decreasing trends are biased. This is particularly clear for low thresholding. Increasing the thresholding (e.g., $\lambda = 4$) improves both peak frequency and trend estimation. It however also leads to over-thresholding for the lower amplitude observed wavelets. Estimations using the Morlet wavelet dictionary seem more sensitive to the amount of thresholding compared to those using the Ricker wavelet dictionary. In the present case, the best compromise is obtained for the Ricker wavelet dictionary with $\lambda = 4$. The corresponding quality factors are close to the theoretical ones (~80 instead of 70 and ~47 instead of 45) even for the last wavelets with low SNR.

4.3. Synchrosqueezing transform

With the SST, we employ either a Ricker or a Morlet mother wavelet with 32 voices per octave and different values of thresholding (i.e., 10, 25, 50 and 80% of the maximum amplitude of continuous wavelet transform time–frequency distributions). Peak frequencies estimated by the SST are consistently higher than the

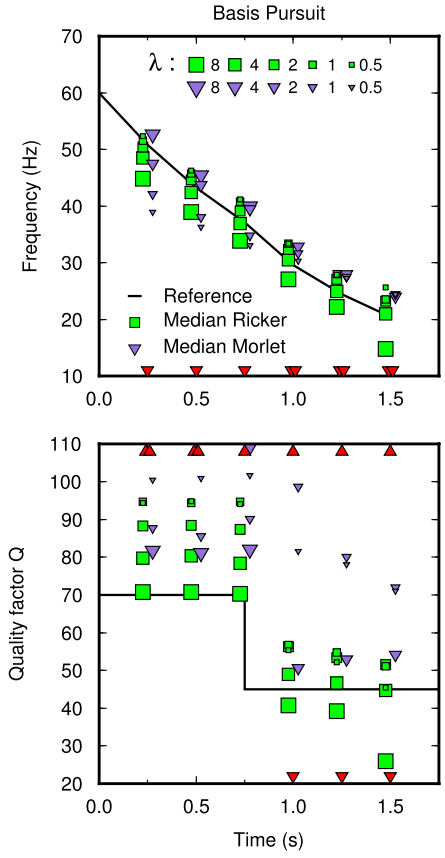

Fig. 3. Median peak frequencies (top) and quality factors (bottom) estimations using basis pursuit (BP) with a Ricker wavelet dictionary (green squares) and a Morlet wavelet dictionary (purple inverted triangles). Symbol sizes depend on the value of the regularization parameter λ. The black lines in the peak frequency (top) and the quality factor (bottom) plots correspond to the reference measurements of the Fourier transform on the noiseless signal (see Table 2) and the theoretical quality factor, respectively. Values outside the figure are indicated by red triangles pointing to their positions. (For interpretation of the references to color in this figure legend, the reader is referred to the web version of this article.)

reference ones (see Table 1 for reference peak frequencies). These peak frequencies are however closer to the reference IFs (Table 3 and Fig. 4).

Using a Ricker mother wavelet, the decreasing trend in peak frequencies is well recovered for the first three wavelets, leading to good quality factor estimations particularly for lower thresholding (thresholding value of 10%, Fig. 4). In most cases, quality factor estimates are however overestimated due to overestimated peak frequencies (see Table 3 and Fig. 1). Intense thresholding (thresholding value of 80%) seems necessary to reduce the noise contribution for the last wavelets which improves the quality factor estimations in these cases (Table 3 and Fig. 4). It also helps reducing the estimated peak frequencies and all the standard deviations.

Table 3
Reference instantaneous frequencies (IF_r) calculated on the noiseless synthetic signal [37] and peak frequencies and quality factors estimations using the synchrosqueezing wavelet transform (SST) with a threshold = 80%. The mother wavelet employed is a Ricker wavelet with 32 voices per octave. See Table 1 for meaning of symbols.

	Reference meas.			SST with thresholding parameter = 80%					
	t (s)	IF_r (Hz)	Q	$\tilde{f}_p$	$\tilde{f}_p$	σ_{f_p}	$\tilde{Q}$	$\tilde{Q}$	σ_Q
f_0	0	67.4							
f_{p1}	0.25	59.2	70	65.8	66.4	5.1	225.9	85.7	841.4
f_{p2}	0.50	52.3	70	56.8	56.9	4.2	86.1	84.4	163.9
f_{p3}	0.75	46.6	70	47.2	47.9	5.4	108.5	88.1	64.8
f_{p4}	1.00	39.3	45	39.7	38.4	6.4	35.7	50.7	213.2
f_{p5}	1.25	33.7	45	30.3	32.3	9.8	88.6	63.0	90.4
f_{p6}	1.50	29.3	45	147.7	33.5	160.8	21.1	2.4	103.7

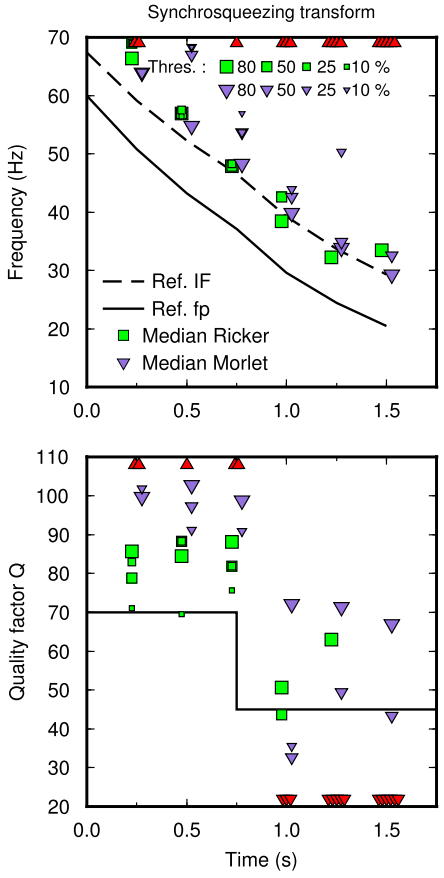

Fig. 4. Median peak frequencies (top) and quality factors (bottom) estimations using the synchrosqueezing wavelet transform (SST) with a Ricker mother wavelet (green squares) and a Morlet mother wavelet (purple inverted triangles), and 32 voices per octave. Symbol sizes depend on the value of the thresholding parameter. Reference peak frequencies, instantaneous frequencies and quality factors are indicated by the black solid line and black dashed line in the peak frequency plot (top), and the black solid line in the quality factor plot (bottom), respectively. Values outside the figure are indicated by red triangles pointing to their positions. (For interpretation of the references to color in this figure legend, the reader is referred to the web version of this article.)

In the case of the Morlet mother wavelet, high thresholding seems necessary in order to obtain consistent estimations. For a threshold of 80%, peak frequency estimates are close to the reference IFs. The pattern in quality factor is also recovered, even though they are overestimated (~100 and ~70 instead of 70 and 45). Even though the pattern of the theoretical quality factors is relatively well conserved by the SST, the actual values are not well recovered in the case of signals with low signal-to-noise ratios.

4.4. Variants of empirical mode decomposition: EEMD and CEEMD

We applied EEMD and CEEMD to the synthetic signal with different combinations of number of iterations (i.e., 15, 100 and 300) and amount of Gaussian white noise (i.e., noise with standard deviations of 5, 10 and 15% of the standard deviation of the signal amplitude). The results using different combinations of these parameters show large and non-systematic variations depending on the set of parameters, and are not shown here. In Table 4, Figs. 6a and 6b we show the best estimates obtained using CEEMD with 100 iterations and 10% of Gaussian white noise. The peak frequencies of the first 4 wavelets are overestimated by about 20–30 Hz, whereas the peak frequencies of the last two wavelets correspond to the random noise.

Results are susceptible to chosen parameter settings (number of iterations and amount of Gaussian white noise) and individual noise realizations. Performing CEEMD twice with the same set of parameters can lead to slightly different signal decompositions [11]. This leads to differences in peak frequencies of up to few Hz in our case. Using CEEMD, the median in estimated peak frequencies follows the true trend, namely a reduction in peak frequency with increasing wavelet number, up to the fourth wavelet. This allows this method to retrieve the pattern in quality factors (Fig. 6). These quality factors are however overestimated by approximately ~20–50%.

5. Discussion

No advanced processing is applied to the synthetic signal presented here. We focus on the performance of the three high-resolution time–frequency transforms regarding the estimation of attenuation. The denoising procedure inherently applied in BP and SST is improving their performance compared with the Fourier transform and CEEMD. Specific processing could be employed depending on the application and the spectral estimation technique such as varying the window length for the FFT depending on the wavelet frequency to reduce the noise contribution.

The peak frequency method requires relatively precise peak frequency measurements in order to provide meaningful quality factors (Fig. 1c). To retrieve the quality factor pattern, small systematic errors are possible as long as the decreasing trend in peak frequencies is conserved. The three time–frequency transforms need some degree of parametrization. BP shows the best performances in terms of precision and robustness, followed by the SST (Figs. 5 and 6).

Peak frequency estimations by BP with a Ricker wavelet dictionary have systematic errors either toward lower frequencies for higher thresholding ($\lambda = 8$) or toward higher frequencies for lower thresholding ($\lambda = 0.5$). These errors are sometimes compensated by the trend in peak frequencies leading to accurate quality factor estimations (e.g., case of $\lambda = 8$ for the first three wavelets). Changing the dictionary for a Morlet wavelet dictionary, which contains wavelets slightly different from the Ricker wavelets used to build the synthetic test signal, leads to a decrease in the accuracy of peak frequencies and quality factors estimates. Obtaining reasonable estimates also requires a different amount of thresholding depending on the dictionary. This difference in behavior for the

Table 4
Reference instantaneous frequencies (IF_r) calculated on the noiseless synthetic signal [37] and peak frequencies and quality factors estimations using the complete ensemble empirical mode decomposition (CEEMD). These results are obtained using 100 iterations and 10% of Gaussian white noise. See Table 1 for meaning of symbols.

	Reference meas.			CEEMD: 100 iter. and 10% Gauss. white noise					
	t (s)	IF_r (Hz)	Q	$\bar{f}_p$	$\tilde{f}_p$	σ_{f_p}	$\bar{Q}$	$\tilde{Q}$	σ_Q
f_{p1}	0.25	59.2	70	78.4	79.9	7.7	92.2	105.2	223.6
f_{p2}	0.50	52.3	70	66.6	68.1	6.9	108.5	108.0	282.3
f_{p3}	0.75	46.6	70	57.5	57.0	5.3	−31.7	104.8	1031.6
f_{p4}	1.00	39.3	45	66.0	52.5	37.1	81.5	52.8	189.6
f_{p5}	1.25	33.7	45	145.4	142.9	19.6	−39.4	−38.1	10.8
f_{p6}	1.50	29.3	45	145.0	142.9	19.3	−59.2	−57.3	16.1

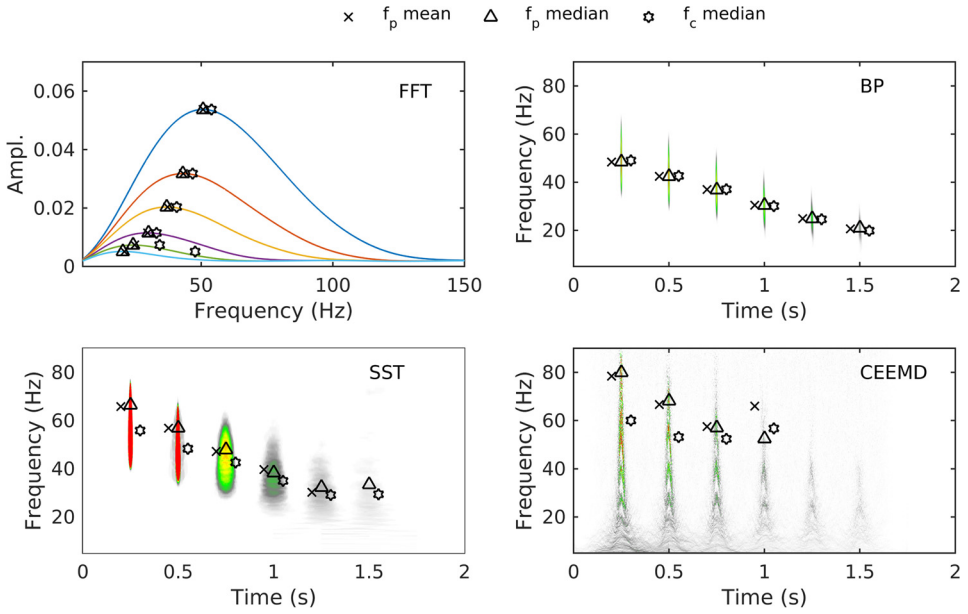

Fig. 5. Fourier spectra (FFT, smoothed spectra) and time–frequency distributions stacked over all noise realizations. Each attenuated wavelet is analyzed individually and then placed at its right time location. For each spectral estimation method, best estimates of mean peak frequencies, median peak frequencies and median centroid frequencies are indicated by black crosses, black triangles and black hexagrams, respectively. The parameters and frequency measures used are those corresponding to Tables 1–4, except for median centroid frequencies of the FFT (Welch spectra plus amplitude threshold) and CEEMD (EEMD using 300 iterations and 5% of Gaussian white noise). Missing values are outside the graphs.

two wavelet dictionaries seems to indicate that the response of the BP algorithm to the noise level and thresholding depends on the wavelet spectral shape. The time–frequency representation of BP, initially based on a representation obtained by the continuous wavelet transform [8], is ultimately a compromise between noise suppression by thresholding and signal preservation during the inversion process.

SST estimations show less resistance to noise compared with BP, resulting in larger standard deviations in peak frequencies and quality factors. The lower performances obtained by the SST arise mainly from the computation of IFs. This leads to peak frequency overestimations which then result in quality factor overestimations. As for BP, changing to a Morlet mother wavelet decreases the accuracy in peak frequency and quality factor estimates. Using a Morlet mother wavelet also seems to increase the sensitivity of SST to the amount of thresholding. Consequently, for both BP and SST, a good estimate of the wavelet in the signal under investigation significantly improves frequency measures and quality factors estimations. The time support of the wavelets of the synthetic signal (∼0.05–0.1 s) may be too small for correct IFs determinations with the SST. An approximate lower bound of this time support is $O(1/f_p)$ [19] leading to 0.017–0.05 s for peak frequencies between 20 and 60 Hz, which is very close to the actual time support of the wavelets. This implies that even new algorithm developments such as the conceFT algorithm [13] or 2D synchrosqueezed transforms [47] might not improve on SST performances in this case.

In this study, we assume that the source spectrum is close to the spectrum of a Ricker wavelet. For many applications, such as seismic applications, this approximation is reasonable even though the true spectrum might slightly differ from a Ricker wavelet spectrum [48]. The relations for quality factor estimation using peak frequencies can also be derived for other wavelet spectra. Applications in combination with highly-localized time–frequency transforms are still restricted to wavelets which can be defined by their peak frequency alone.

The computation of IFs for CEEMD also results in large peak frequency overestimations as well as a variance increase in frequency measures. Potential spurious IMFs together with the introduction of some random noise to the IMFs also contribute to increase this estimation variance [11], subsequently increasing the uncertainty in derived quality factors. This, in combination with a low resistance to background noise, limit the application of CEEMD to attenuation measurements. The analytical signal method for attenuation measurement uses directly IFs [14]. This might be more suitable to CEEMD even though this method also requires a very accurate selection of each wavelet time support [42].

In Fig. 6b, we also compare quality factor estimates obtained using the peak frequency method in combination with high-resolution techniques with those obtained using the frequency shift and spectral ratio methods [33]. To compute quality factors using these methods, we employ smoothed Fourier spectra together with amplitude thresholds specific to each wavelet. Qual-

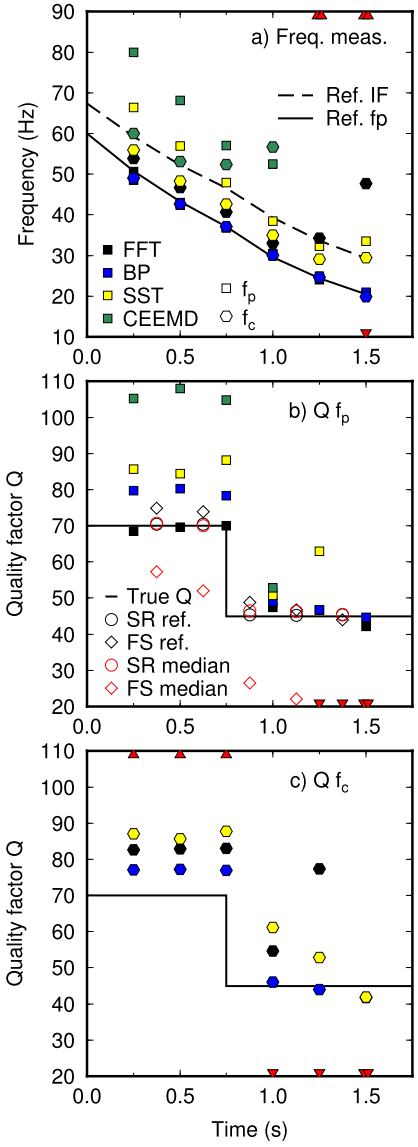

Fig. 6. a) Best median peak frequency (f_p, squares) and frequency centroid (f_c, hexagons) measurements for the FFT (black), BP (blue), the SST (yellow) and CEEMD (green). The parameters used are those of Tables 1–4, except for frequency centroid measurements by the FFT (Welch spectra plus amplitude threshold) and CEEMD (EEMD using 300 iterations and 5% of Gaussian white noise). b) and c) Quality factor estimates using peak frequencies and frequency centroids, respectively, and the same set of parameters as in a). Quality factor estimates using the spectral ratio (SR, circles) and frequency shift (FS, diamonds) methods are also shown for the noise-free synthetic signal (SR and FS ref. in black) and the noisy signals (median values: SR and FS median in red). The true quality factors are indicated by the black line. Values outside the figure are indicated by red triangles pointing to their positions. (For interpretation of the references to color in this figure legend, the reader is referred to the web version of this article.)

ity factors are computed for all noise realizations and the median value is retained and presented in Fig. 6b. Quality factor estimates from the spectral ratio method are accurate even for the last wavelets with low SNR. On the other hand, estimates from the frequency shift are biased due to the presence of noise and the need of an amplitude threshold. Overall, for this synthetic signal example, quality factor estimates using the peak frequency estimate with the high-resolution time–frequency techniques are generally less accurate than those of the spectral ratio method but on par or better than those of the frequency shift method.

Instead of using peak frequencies, we also tested using frequency centroids. The frequency centroid f_c of an amplitude spectrum $A(f)$ is given by

$$f_c = \frac{\int_0^\infty f A(f)\,\mathrm{d}f}{\int_0^\infty A(f)\,\mathrm{d}f}. \tag{12}$$

In principle, parts of the spectra are lost for highly-localized time–frequency transforms which may bias the estimation of frequency centroids. However, BP and the SST show similar or better results using frequency centroids. This means that these three time–frequency representations are effectively concentrated around the peak frequencies and that the decreasing trend in frequency is conserved (Fig. 6). In details, BP results using frequency centroids are similar to those using peak frequencies in terms of accuracy, but slightly better in terms of standard deviations. For the SST, frequency centroids are approximately 5–10 Hz lower than peak frequencies. It clearly improves frequency and quality factor estimations for the last wavelets and reduce standard deviations in most cases. On the other hand, CEEMD results using frequency centroids worsen with estimated quality factors around 150 and negative for the first three and last three wavelets, respectively. This could arise from the contamination of the main IMF carrying the wavelet by other IMFs containing mainly noise.

In the case of real data, this method can be applied on wavelets at specific times/distances. A decreasing trend in frequency bandwidth over time is generally observed for seismic traces [23]. Frequency centroids or peak frequencies could then be measured in a sliding window and over the entire signal [15]. These "effective quality factors" can be used directly for attenuation compensation [44]. On the other hand, prior information, inversion schemes, and/or peak frequencies picking [49] could be used to define potential layers or structures to determine layer quality factors. Layer quality factors distribution can then be compared with known structures distribution for interpretation [35]. The combination of high-resolution time–frequency transforms with attenuation measurements represents another strategy to reduce noise interferences compared with inversion schemes (e.g., [34]) or the development of more robust frequency measures (e.g., [30]).

6. Conclusion

Conventional attenuation measurement techniques, such as spectral ratios and the frequency shift method, compare large spectral bandwidth to estimate attenuation. As a consequence, high-resolution time–frequency transforms cannot be employed due to the high localization of their time–frequency distributions. Based on the assumption that the source wavelet is approximated by a Ricker wavelet with a spectrum fully defined through its peak frequency, the peak frequency method for attenuation measurement only requires an accurate estimation of peak frequencies or frequency centroids and their trend over time.

The three time–frequency transforms: BP, the SST and CEEMD, tested on a noisy synthetic signal, are able to retrieve this trend but show different performances in terms of dominant frequency estimations. Estimations based on BP are more accurate and robust compared with those of the SST and CEEMD. BP estimations rely mainly on the determination of a compromise between thresholding and signal preservation. For BP and SST, using an inappropriate wavelet template decreases the quality of quality factor estimates; yet decomposition results are insensitive to small differences between the employed wavelet template and the true source wavelet. For SST and CEEMD, estimated peak frequencies are overestimated due to the use of IFs. In the case of CEEMD, some Gaussian white noise is also injected as part of the signal decomposition process into IMFs, which lead to significant fluctuations in dominant frequency estimates. For SST, the wavelets time support in the synthetic benchmarking example is close to the lower bound for good

IFs determination. Using frequency centroids instead of peak frequencies includes some smoothing which benefits SST estimation of dominant frequencies, particularly in the case of wavelets with lower signal-to-noise ratios. Comparison with the two conventional methods for quality factor estimation shows that the peak frequency method with high-resolution transforms has results slightly less accurate than those of the spectral ratio method, and similar or better than those of the frequency shift method in our example. This analysis shows that despite their discontinuous spectra, highly-localized time–frequency transforms have applications for attenuation measurements in geophysics or other fields.

Acknowledgments

The authors would like to thank the sponsors of the Microseismic Industry consortium for financial support, and Haizhao Yang and Hau-tieng Wu for thoughtful discussions. We thank three anonymous reviewers for their constructive comments. We also acknowledge the authors of the original codes for the synchrosqueezing transform (synchrosqueezing transform toolbox, https://web.math.princeton.edu/~ebrevdo/synsq/), empirical mode decomposition (P. Flandrin, http://perso.ens-lyon.fr/patrick.flandrin/emd.html, M.E. Torres, http://bioingenieria.edu.ar/grupos/ldnlys/metorres/re_inter.htm, and J. Han), and basis pursuit (M. Sacchi, D. Bonar and I. Vera Rodriguez).

References

[1] B. Barnhart, W. Eichinger, Analysis of sunspot variability using the Hilbert–Huang transform, Sol. Phys. 269 (2) (2011) 439–449, http://dx.doi.org/10.1007/s11207-010-9701-6.
[2] D.C. Bauer, C.C. Glüer, J.A. Cauley, et al., Broadband ultrasound attenuation predicts fractures strongly and independently of densitometry in older women: a prospective study, Arch. Intern. Med. 157 (6) (1997) 629–634, http://dx.doi.org/10.1001/archinte.1997.00440270067006.
[3] A. Beck, M. Teboulle, A fast iterative shrinkage–thresholding algorithm for linear inverse problems, SIAM J. Imaging Sci. 2 (1) (2009) 183–202.
[4] M. Bekara, M. van der Baan, Random and coherent noise attenuation by empirical mode decomposition, Geophysics 74 (5) (2009) V89–V98, http://dx.doi.org/10.1190/1.3157244.
[5] A. Best, C. McCann, J. Sothcott, The relationships between the velocities, attenuations and petrophysical properties of reservoir sedimentary rocks, Geophys. Prospect. 42 (2) (1994) 151–178, http://dx.doi.org/10.1111/j.1365-2478.1994.tb00204.x.
[6] T.D. Blanchard, P. Delommot, An example of the measurement and practical applications of time-lapse seismic attenuation, Geophysics 80 (2) (2015) WA25–WA34, http://dx.doi.org/10.1190/geo2014-0186.1.
[7] D. Bonar, M. Sacchi, Complex spectral decomposition via inversion strategies, in: SEG Annual Meeting, vol. 29, 2010, pp. 1408–1412.
[8] D. Bonar, M. Sacchi, Spectral decomposition with f–x–y preconditioning, Geophys. Prospect. 61 (2013) 152–165, http://dx.doi.org/10.1111/j.1365-2478.2012.01104.x.
[9] M. Chekroun, L.L. Marrec, O. Abraham, O. Durand, G. Villain, Analysis of coherent surface wave dispersion and attenuation for non-destructive testing of concrete, Ultrasonics 49 (8) (2009) 743–751, http://dx.doi.org/10.1016/j.ultras.2009.05.006.
[10] S.S. Chen, D.L. Donoho, M.A. Saunders, Atomic decomposition by basis pursuit, SIAM Rev. 1 (2001) 129–159.
[11] M.A. Colominas, G. Schlotthauer, M.E. Torres, Improved complete ensemble EMD: a suitable tool for biomedical signal processing, Biomed. Signal Process. Control 14 (2014) 19–29, http://dx.doi.org/10.1016/j.bspc.2014.06.009.
[12] I. Daubechies, J. Lu, H.-T. Wu, Synchrosqueezed wavelet transforms: an empirical mode decomposition-like tool, Appl. Comput. Harmon. Anal. 30 (2) (2011) 243–261, http://dx.doi.org/10.1016/j.acha.2010.08.002.
[13] I. Daubechies, Y. Wang, H.-T. Wu, ConceFT: concentration of frequency and time via a multitapered synchrosqueezed transform, preprint, arXiv:1507.05366, 2015.
[14] L. Engelhard, Determination of seismic-wave attenuation by complex trace analysis, Geophys. J. Int. 125 (2) (1996) 608–622, http://dx.doi.org/10.1111/j.1365-246X.1996.tb00023.x.
[15] M. Fink, F. Hottier, J. Cardoso, Ultrasonic signal processing for in vivo attenuation measurement: short time Fourier analysis, Ultrason. Imag. 5 (2) (1983) 117–135, http://dx.doi.org/10.1016/0161-7346(83)90014-7.
[16] P. Flandrin, G. Rilling, P. Gonçalvés, Empirical mode decomposition as a filter bank, IEEE Signal Process. Lett. 11 (2) (2004) 112–114, http://dx.doi.org/10.1109/LSP.2003.821662.
[17] G. Ghoshal, M.L. Oelze, Time domain attenuation estimation method from ultrasonic backscattered signals, J. Acoust. Soc. Am. 132 (1) (2012) 533–543.
[18] Y. Haizhao, Synchrosqueezed wave packet transforms and diffeomorphism based spectral analysis for 1D general mode decompositions, Appl. Comput. Harmon. Anal. 39 (1) (2015) 33–66.
[19] Y. Haizhao, Y. Lexing, Synchrosqueezed curvelet transform for two-dimensional mode decomposition, SIAM J. Math. Anal. 46 (3) (2014) 2052–2083, http://dx.doi.org/10.1137/130939912.
[20] J. Han, M. van der Baan, Empirical mode decomposition for seismic time–frequency analysis, Geophysics 78 (2) (2013) O9–O19.
[21] K. Haneca, K. Deforce, M.N. Boone, D. Van Loo, M. Dierick, J. Van Acker, J. Van den Bulcke, X-ray sub-micron tomography as a tool for the study of archaeological wood preserved through the corrosion of metal objects, Archaeometry 54 (5) (2012) 893–905, http://dx.doi.org/10.1111/j.1475-4754.2011.00640.x.
[22] C.M. Harris, Absorption of sound in air versus humidity and temperature, J. Acoust. Soc. Am. 40 (1) (1966) 148–159, http://dx.doi.org/10.1121/1.1910031.
[23] R.H. Herrera, J. Han, M. van der Baan, Applications of the synchrosqueezing transform in seismic time–frequency analysis, Geophysics 79 (3) (2014) V55–V64, http://dx.doi.org/10.1190/geo2013-0204.1.
[24] R.H. Herrera, J.B. Tary, M. van der Baan, D.W. Eaton, Body wave separation in the time–frequency domain, IEEE Geosci. Remote Sens. Lett. 12 (2) (2015) 364–368, http://dx.doi.org/10.1109/LGRS.2014.2342033.
[25] N.E. Huang, Z. Shen, S.R. Long, M.C. Wu, H.H. Shih, Q. Zheng, N.-C. Yen, C.C. Tung, H.H. Liu, The empirical mode decomposition and the Hilbert spectrum for nonlinear and non-stationary time series analysis, Proc. R. Soc. Lond. A 454 (1998) 903–995, http://dx.doi.org/10.1098/rspa.1998.0193.
[26] Z.-L. Huang, J. Zhang, T.-H. Zhao, Y. Sun, Synchrosqueezing S-transform and its application in seismic spectral decomposition, IEEE Trans. Geosci. Remote Sens. 54 (2) (2016) 817–825, http://dx.doi.org/10.1109/TGRS.2015.2466660.
[27] B. Jones, D. Stone, Towards an ultrasonic-attenuation technique to measure void content in carbon-fibre composites, Non-Destruct. Test. 9 (2) (1976) 71–79, http://dx.doi.org/10.1016/0029-1021(76)90004-9.
[28] U. Katz, C. Spiering, High-energy neutrino astrophysics: status and perspectives, Prog. Part. Nucl. Phys. 67 (3) (2012) 651–704, http://dx.doi.org/10.1016/j.ppnp.2011.12.001.
[29] L. Knopoff, Q, Rev. Geophys. 2 (4) (1964) 625–660, http://dx.doi.org/10.1029/RG002i004p00625.
[30] F. Li, H. Zhou, N. Jiang, J. Bi, K.J. Marfurt, Q estimation from reflection seismic data for hydrocarbon detection using a modified frequency shift method, J. Geophys. Eng. 12 (4) (2015) 577–586, http://dx.doi.org/10.1088/1742-2132/12/4/577.
[31] S. Mallat, A Wavelet To ur of Signal Processing: The Sparse Way, third edition, Academic Press, 2008.
[32] T.M. Müller, B. Gurevich, M. Lebedev, Seismic wave attenuation and dispersion resulting from wave-induced flow in porous rocks – a review, Geophysics 75 (5) (2010) 75A147–75A164.
[33] Y. Quan, J.M. Harris, Seismic attenuation tomography using the frequency shift method, Geophysics 62 (3) (1997) 895–905, http://dx.doi.org/10.1190/1.1444197.
[34] C. Reine, R. Clark, M. van der Baan, Robust prestack Q-determination using surface seismic data, part 1: method and synthetic examples, Geophysics 77 (1) (2012) R45–R56.
[35] C. Reine, R. Clark, M. van der Baan, Robust prestack Q-determination using surface seismic data, part 2: 3D case study, Geophysics 77 (1) (2012) B1–B10, http://dx.doi.org/10.1190/geo2011-0074.1.
[36] B. Schurr, G. Asch, A. Rietbrock, R. Trumbull, C. Haberland, Complex patterns of fluid and melt transport in the central Andean subduction zone revealed by attenuation tomography, Earth Planet. Sci. Lett. 215 (1) (2003) 105–119.
[37] M.T. Taner, F. Koehler, R. Sheriff, Complex seismic trace analysis, Geophysics 44 (6) (1979) 1041–1063.
[38] J.B. Tary, R.H. Herrera, J. Han, M. van der Baan, Spectral estimation – what is new? What is next?, Rev. Geophys. 52 (2014) 723–749, http://dx.doi.org/10.1002/2014RG000461.
[39] G. Thakur, H.-T. Wu, Synchrosqueezing-based recovery of instantaneous frequency from nonuniform samples, SIAM J. Math. Anal. 43 (5) (2011) 2078–2095.
[40] G. Thakur, E. Brevdo, N.S. Fučkar, H.-T. Wu, The synchrosqueezing algorithm for time-varying spectral analysis: robustness properties and new paleoclimate applications, Signal Process. 93 (5) (2013) 1079–1094, http://dx.doi.org/10.1016/j.sigpro.2012.11.029.
[41] D. Thomson, Spectrum estimation and harmonic analysis, Proc. IEEE 70 (9) (1982) 1055–1096, http://dx.doi.org/10.1109/PROC.1982.12433.
[42] R. Tonn, The determination of the seismic quality factor Q from VSP data: a comparison of different computational methods, Geophys. Prospect. 39 (1) (1991) 1–27, http://dx.doi.org/10.1111/j.1365-2478.1991.tb00298.x.
[43] M. Torres, M. Colominas, G. Schlotthauer, P. Flandrin, A complete ensemble empirical mode decomposition with adaptive noise, in: 2011 IEEE Interna-

tional Conference on Acoustics, Speech and Signal Processing, ICASSP, 2011, pp. 4144–4147.
[44] M. van der Baan, Bandwidth enhancement: inverse Q filtering or time-varying Wiener deconvolution?, Geophysics 77 (4) (2012) V133–V142, http://dx.doi.org/10.1190/geo2011-0500.1.
[45] I. Vera Rodriguez, D. Bonar, M. Sacchi, Microseismic data denoising using a 3C group sparsity constrained time–frequency transform, Geophysics 77 (2) (2012) V21–V29.
[46] Z. Wu, N.E. Huang, Ensemble empirical mode decomposition: a noise-assisted data analysis method, Adv. Adapt. Data Anal. 1 (1) (2009) 1–41, http://dx.doi.org/10.1142/S1793536909000047.
[47] H. Yang, Robustness analysis of synchrosqueezed transforms, preprint, arXiv:1410.5939, 2014.
[48] C. Zhang, T.J. Ulrych, Estimation of quality factors from CMP records, Geophysics 67 (5) (2002) 1542–1547, http://dx.doi.org/10.1190/1.1512799.
[49] C. Zhang, T.J. Ulrych, Seismic absorption compensation: a least squares inverse scheme, Geophysics 72 (6) (2007) R109–R114, http://dx.doi.org/10.1190/1.2766467.
[50] R. Zhang, J. Castagna, Seismic sparse-layer reflectivity inversion using basis pursuit decomposition, Geophysics 76 (6) (2011) R147–R158.

Jean Baptiste Tary received an M.Sc. (2007) from the Joseph Fourier University, France, and a Ph.D. (2011) from the Western Brittany University and IFREMER institute, France, in geophysics. He was a postdoctoral fellow at the University of Alberta, Canada, from 2011 to 2013 and in 2015, working for the Microseismic Industry Consortium. In 2014, he was a postdoctoral fellow at the University of Vienna working on earthquake interactions, and is now an assistant professor at the Universidad de los Andes, Colombia. His research interests include time–frequency transforms applications, resonance phenomena, seismic attenuation and relationships between fluids and Earth's deformation.

Mirko van der Baan is a professor at the University of Alberta in the Department of Physics, specializing in Exploration Seismology. He graduated in 1996 from the University of Utrecht in the Netherlands, obtained a PhD with honors in 1999 from the Joseph Fourier University, France, and then joined the University of Leeds, UK, where he became the Reader of Exploration Seismology. He also holds an HDR (Habilitation) from University Denis Diderot, France. He is currently the Director of the Microseismic Industry Consortium, a collaborative venture with the University of Calgary, dedicated to research in microseismicity. He is a member of the editorial board of Geophysics.

Roberto Henry Herrera received a B.Sc. (1995) and M.Sc. (1998) in electronics and telecommunications and a Ph.D. in signal processing (2007) all from UCLV, Cuba. He was a postdoctoral fellow at the University of Alberta, Canada from 2010 to 2014, working on signal processing topics for the Blind Separation of Seismic Signals (BLISS) project and the Microseismic Industry Consortium. His research interests include statistical signal processing, exploratory data analysis, time–frequency transforms and pattern recognition. He serves as a reviewer for several journals and is an IEEE Senior member.